ACS Sustainable Chemistry & Engineering

Research Article

pubs.acs.org/journal/ascecg

Novel Synthesis and Characterization of Mesoporous ZnO Nanofibers by Electrospinning Technique

Sawanta S. Mali,[†] Hyungjin Kim,[†] Woon Yeong Jang,[†] Hye Seon Park,[†] Pramod S. Patil,[†,‡] and Chang Kook Hong*[,†]

[†]Advanced Chemical Engineering Department, Chonnam National University, Gwangju 500-757, South Korea

[‡]Thin Film Materials Laboratory, Department of Physics, Shivaji University, Kolhapur-416004, India

ABSTRACT: Wurzite type zinc oxide (ZnO) mesoporous nanofibers for low-cost thin film solar cells were successfully synthesized by a simple electrospinning technique. The n-type semiconducting ZnO mesoporous nanofibers were obtained from polyvinylpyrrolidone (PVP) and a zinc nitrate precursor in ethanol and water after calcination treatment at 520 °C for 1 h. The as-synthesized PVP−ZnO and calcined ZnO nanofibers were characterized using X-ray powder diffraction (XRD), thermogravimetric analysis (TGA), scanning electron microscopy (SEM), transmission electron microscopy (TEM), and X-ray photoelectron spectroscopy (XPS). The vibrational properties of the ZnO mesoporous nanofibers were recorded by micro-Raman spectroscopy. The results show that the calcined ZnO mesoporous nanofibers have a single phase with good crystallinity.

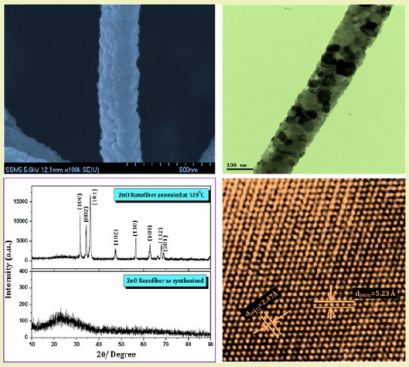

KEYWORDS: *Mesoporous ZnO nanofibers, HRTEM, XPS, Raman*

INTRODUCTION

Recently, 1D nanorods, nanoflowers, nanowires, and nanofibers of zinc oxide (ZnO) have shown great potentials due to having promising photocatalysts for high catalytic activity and for being excellent candidates for dye sensitized solar cells (DSSC)[1] and quantum dot-sensitized solar cells (QDSSC).[2] The ZnO favors formation of anisotropic structures and exhibits much higher electron mobility than titanium oxide (TiO_2) (155 $cm^2\ V^{-1}\ s^{-1}$ vs 10^{-5} $cm^2\ V^{-1}\ s^{-1}$). The Debye−Huckel screening length in ZnO is about 4 nm for a carrier concentration of 10^{18} cm^{-3}. They also have high exciton binding energy (60 meV), high breakdown strength, and exciton stability, and are an environmentally friendly material.[3−5] The electron concentration (n) and electron mobility (μ_e) in the single crystalline ZnO nanofibers synthesized by electrospinning is 1.3×10^{19} cm^{-3} and 4.6×10^{-3} $cm^2V^{-1}s^{-1}$,respectively.[6] The μ_e of bulk ZnO is 205−300 $cm^2\ V^{-1}\ s^{-1}$, while a single nanowire shows 1000 $cm^2\ V^{-1}\ s^{-1}$ electron mobility.[7] In the case of TiO_2, nanopartcles and nanorods have 0.1−4 $cm^2\ V^{-1}\ s^{-1}$ electron mobility, which is much smaller than either bulk or single crystalline ZnO. The electron diffusion coefficient of bulk ZnO is 5.2 $cm^2\ s^{-1}$ and 1.7×10^{-4} $cm^2\ s^{-1}$ for nanoparticulate film.[7,8] The electron diffusion coefficients of bulk and nanoparticulate TiO_2 are 0.5 $cm^2\ s^{-1}$ and 10^{-8}−10^{-4} $cm^2\ s^{-1}$, respectively.[9,10] The highest room-temperature electron mobility for a bulk ZnO single crystal grown by the vapor-phase transport method is reported to be about 205 $cm^2\ V^{-1}\ s^{-1}$ with a carrier concentration of 6.0×10^{16} cm^{-3}.[11,12] From the above discussion, it is clear that ZnO has higher electronic mobility that would be favorable for effective electron transport and low recombination loss when used in DSSCs/QDSSCs.

A number of approaches have been employed for the synthesis of ZnO, which include physical vapor deposition (PVD),[13] chemical vapor deposition (CVD),[14] molecular beam epitaxy (MBE),[15] metal-organic chemical vapor deposition (MOCVD),[16] thermal evaporation,[17] combustion method,[18] aqueous chemical growth (ACG),[19] and hydrothermal.[20] On the other hand, 1D ZnO nanostructures like nanowires/nanofibers are receiving increasing attention because of their large length to diameter ratios, high surface area, excellent aspect ratio, and effective electronic properties. These properties are making ZnO a promising candidate for DSSC/QDSSc, photocatalysis, and related applications.[21] The ZnO nanowires/nanofibers are mainly synthesized by two different routes, which include the vapor-phase route and solution-processed route. So far, ZnO nanowires/nanofibers synthesized by the vapor-phase route include MOCVD,[22] CVD,[23] PVD,[24] pulsed laser deposition (PLD),[25] metal organic vapor-phase epitaxy (MOVPE),[26] and MBE.[27] Yu et al. synthesized metal catalyst seed-free ZnO nanowires by using the vapor-phase transport deposition technique directly onto a fluorine-doped tin oxide (FTO)-coated substrate.[28]

Recently Ho et al. developed multi-junction ZnO nanowire arrays using a chemical process. These multi-junction ZnO nanowires facilate enhanced surface areas and effective light

Received: May 21, 2013
Revised: June 21, 2013
Published: June 25, 2013

trapping in the DSSC application.[29] Bulovic et al. developed ZnO NW arrays using sol−gel ZnO seeding followed by a low-temperature aqueous chemical route. These nanowire arrays are very beneficial for PbS-sensitized QDSSCs.[30] Zhu et al. synthesized aligned ZnO by using the electrospun technique for ultraviolet nanosensors using polyvinylpyrrolidone (PVP) in dimethyl formamide annealed at 500 °C to remove organic compounds.[31]

Presently, the electrospinning preparation of 1D nanofibers consists of a simple process that can produce a number of different synthetic fibers that show considerable potential for practical applications. The commonly used PVP acts as a mesopore template. It has good electrospinnability and can generated single fluid electrospinning, which is a popular procedure for producing nanofibers due to ease of implementation and cost effectiveness.[32] Initially, the electrospinning is a method of producing fibers by accelerating a jet of charged PVP polymer solution in an electric field.[33] A high-voltage 15 kV power supply generates an electric field between a syringe with a needle tip and a grounded collector drum covered with aluminum foil. Electrostatic charging of the fluid at the needle tip of the syringe results in formation of the well-known Taylor cone, and single fluid jet is ejected from the apex.[34] As the jet accelerates and thins in the electric field, radial charge repulsion results in splitting of the primary jet into multiple filaments. The PVP−ZnO composite filaments were formed from the solution between two electrodes bearing electrical charges of opposite polarity. Finally, these PVP−ZnO fibers are collected on the surface of a collector. Moreover, PVP is a nontoxic, odorless, and environmentally benign polymer, which is widely used as a functional material in various fields,[35] and thus, it is an excellent organic component for use in the synthesis of organic−inorganic hybrid composites. Because of its excellent solubility in alcohol and suitability for ZnO precursors, we have selected the PVP binder in an electrospinning technique. This study reports the successful synthesis of ZnO nanofibers via an electrospinning process, and ZnO mesoporous nanofibers can then be obtained once these have been subject to annealing treatment at 520 °C for 1 h.

EXPERIMENTAL SECTION

Chemicals and Materials. Zinc nitratehexahydrate [$Zn(NO_3)_2 \bullet 6H_2O$] and polyvinylpyrrolidone (PVP) ((PVP K90, M_W = 1,300,000) were purchased from Sigma Aldrich. The solvent ethanol was purchased from Daejung Chemical. Deionized (DI) water was used for the precursor solvent. All these chemicals were used without further purification.

Preparation OF ZnO Feeding Solution. In a typical experiment, a 1:0.75 ratio of zinc nitrate and PVP was dissolved in 7.5:2.5 v:v of ethanol and DI water solvent under magnetic stirring to obtain a homogeneous precursor of ZnO. The prepared PVP−ZnO electrospinning solution was carefully sucked into a 5 mL glass syringe and fixed horizontally arranged by the electrospinning equipment (SGE Analytical Science). The positive electrode was connected to the needle of the syringe containing the precursor solution. The drum rotating speed (400 rpm) and distance between anode and cathode (15 cm) were kept constant. The applied potential was maintained at 15 kV. The feeding rate and drum rotating speed were kept constant at 1.0 mL/h (syringe pump (KDS-100, KD Scientific) and 400 rpm, respectively. The electrospinning deposition was conducted in air. The PVP−ZnO nanofibers were electrospun on aluminum foil. The obtained PVP−ZnO nanofibers were calcined at 520 °C for 1 h (heating rate: 2 °C min^{-1}) using a programmable furnace to get pure mesoporous ZnO nanofibers. The calcined ZnO nanofibers were used for further characterizations.

Characterizations. X-ray diffraction (XRD) measurements were carried out using a D/MAX Uitima III XRD spectrometer (Rigaku, Japan) with a Cu Kα line of 1.5410 Å. The surface morphology of the prepared PVP−ZnO and calcined mesoporous ZnO nanofiber samples were recorded by a field emission scanning electron microscope (FESEM; S-4700, Hitachi). Transmission electron microscopy (TEM) micrographs, selected area electron diffraction (SAED) pattern, and high-resolution transmission electron microscopy (HRTEM) images were obtained by a TECNAI F20 Philips operated at 200 KV. The TEM sample was prepared by drop casting ethanolic dispersion of ZnO nanofibers onto a carbon-coated Cu grid. The elemental information of calcined ZnO nanofibers was analyzed using a X-ray photoelectron spectrometer (XPS) (VG Multilab 2000-Thermo Scientific, U.S.A., K-Alpha) with a multi-channel detector, which can endure high photonic energies from 0.1 to 3 keV. Thermal analysis was carried out with a Shimadzu-TGA-50 TG-DTA thermal analyzer in a nitrogen atmosphere at a heating rate of 10 °C min^{-1}. The micro-Raman spectrum of the ZnO nanofibers was recorded in the spectral range of 100−1000 cm^{-1} using a micro-Raman spectrometer (inVia Reflex UV Raman microscope (Renishaw, U.K.), KBSI, Gwangju-center) that employs a He−Ne laser source with an excitation wavelength 633 nm and resolution of 1 cm^{-1} at 15 mW laser power.

RESULTS AND DISCUSSION

The crystalline structure of the PVP−ZnO fibers and ZnO mesoporous nanofibers have been studied based on their X-ray diffraction patterns obtained at 15 kV. Figure 1 shows the XRD

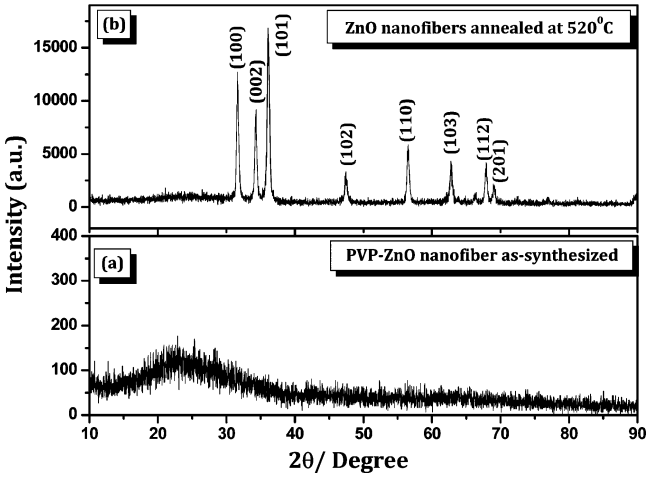

Figure 1. XRD patterns of (a) as-synthesized PVP-ZnO nanofibers and (b) after annealing at 520 °C.

patterns of as-synthesized pure PVP−ZnO nanofibers and after calcination at 520 °C for 1 h. From the XRD pattern, it is clear that the as-prepared PVP−ZnO nanofibers are amorphous in nature. This XRD pattern indicates that the crystalline ZnO structures did not form at room temperature. Therefore, we have calcined PVP−ZnO samples at 520 °C. Figure 1(b) shows the PVP−ZnO nanofibers annealed at 520 °C for 1 h. The peaks are quite sharper, indicating the crystalline nature. The calcined ZnO nanofiber sample (Figure 1(b)) shows nine diffraction peaks of the ZnO mesoporous nanofibers corresponding to (110), (002), (101), (102), (110), (103), (200), (112), and (201) at 31.60°, 34.318°, 36.08°, 47.38°, 56.48°, 62.74°, 66.474°, 67.90°, and 69.04°, respectively, of the wurtzite crystal structure. All diffraction peaks that are consistent with the reported data confirm ZnO with a wurtzite hexagonal phase. No characteristic peaks for other impurities were observed, which confirms that the product obtained after

Table 1. Standard and Observed *d* Values and Their Relative Intensities of ZnO Mesoporous Nanofibers

sr. no.	2θ (standard)	2θ (observed)	(hkl) plane	standard d (Å) a = 3.2498 c = 5.2066	observed d (Å)a = 3.2526 c = 5.2054	standard relative intensity I/I_0 (%)	observed relative intensity I/I_0 (%)
1	31.769	31.602	100	2.8143	2.8288	57	73.90
2	35.421	34.318	002	2.6033	2.6109	44	51.90
3	36.252	36.081	101	2.4759	2.4873	100	100.00
4	47.538	47.383	102	1.9111	1.9170	23	19.62
5	56.602	56.481	110	1.6247	1.6279	32	32.80
6	62.862	62.743	103	1.4771	1.4797	29	25.10
7	66.378	66.474	200	1.4070	1.4054	4	5.50
8	67.961	67.901	112	1.3781	1.3793	21	22.50
9	69.098	69.040	201	1.3582	1.3592	11	11.35
10	76.953	77.076	202	1.2380	1.2363	4	3.20
11	89.609	89.800	203	1.0931	1.0912	7	6.60

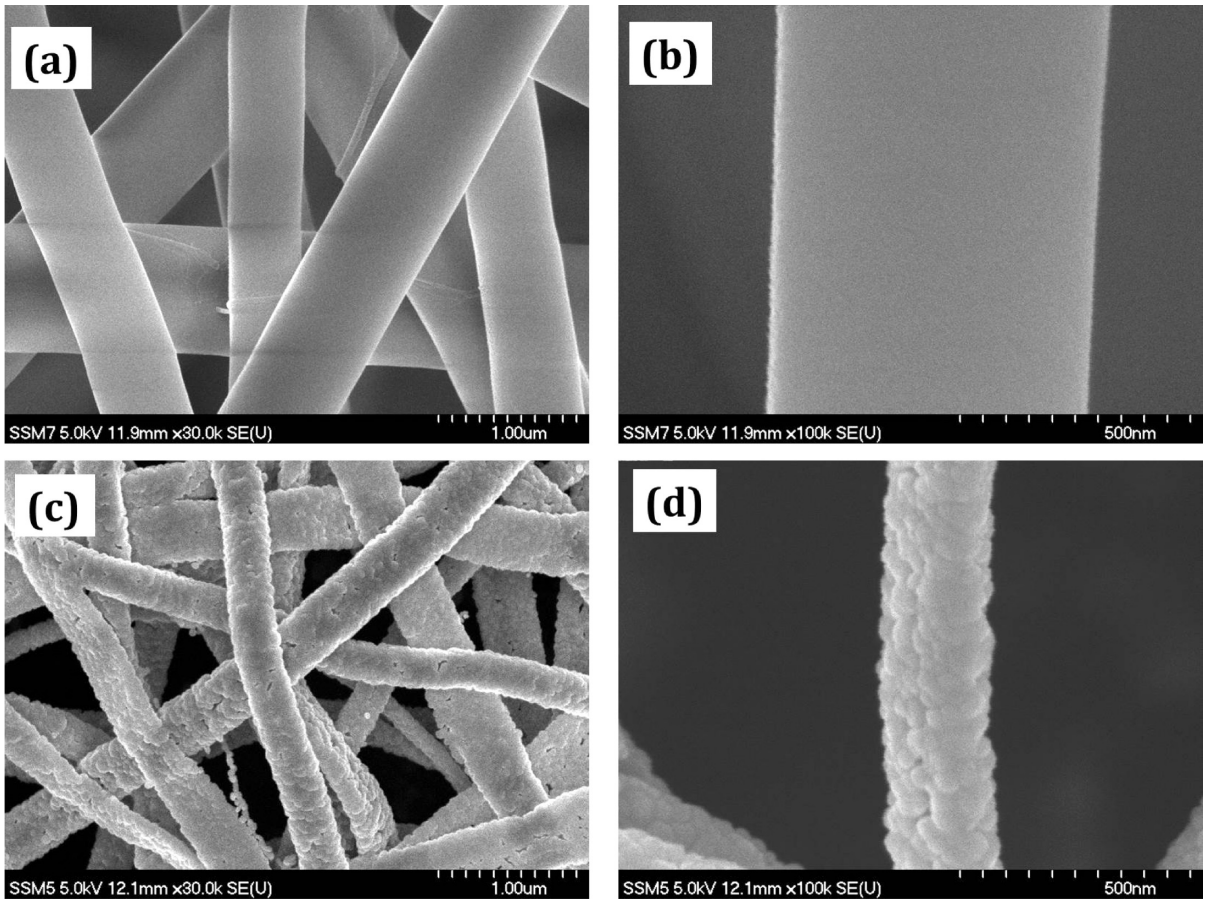

Figure 2. (a, b) FESEM images of as synthesized PVP−ZnO nanofibers and (c, d) after annealing at 520 °C.

calcination is phase pure. The mean values of a = 3.2526 Å and c = 5.2054 Å are in good accord with the reported values (a = 3.2498 Å and c = 5.2066 Å).[3] The XRD observations suggest that the calcination process can play a role to remove the PVP from the as-synthesized sample and improve the crystallinity of ZnO nanofibers. The measured c/a ratio of 1.60 showed a good match with the value 1.605 for an ideally close-packed hexagonal {P63mc(186)} structure obtained from the standard JCPDS data 36-1451. The average crystal domain size of the ZnO mesoporous nanofibers calculated using Scherrer's equation based on the (101) peak is 24 nm ($D = k\lambda/(\beta \cos \theta)$; k = 0.89, λ =1.54 Å, β = fwhm, θ = diffraction angle). The observed and standard crystallographic data is summarized in Table 1.

Figure 2(a) shows the FESEM image of the as-synthesized ZnO nanofibers. From the FESEM image, it is clear that all PVP−ZnO nanofibers are uniform in diameter. The higher magnified FESEM image shows that the PVP−ZnO nanofibers have diameters of about 400 nm and lengths up to several hundreds of micrometers, which indicates that electrospinning is an excellent technique for synthesis of long ZnO nanofibers. The higher magnified FESEM image reveals that the surfaces of ZnO nanofibers are quite smooth (as shown in Figure 2(b)). In the electrospinning process, the PVP is used to adjust the solution viscosity, and ethanol was added to dissolve the PVP and to facilitate the solvent evaporation during the electrospinning process. Also, ethanol plays an important role in local polarization in the solution during electrospinning. These

dx.doi.org/10.1021/sc400153j | ACS Sustainable Chem. Eng. 2013, 1, 1207−1213

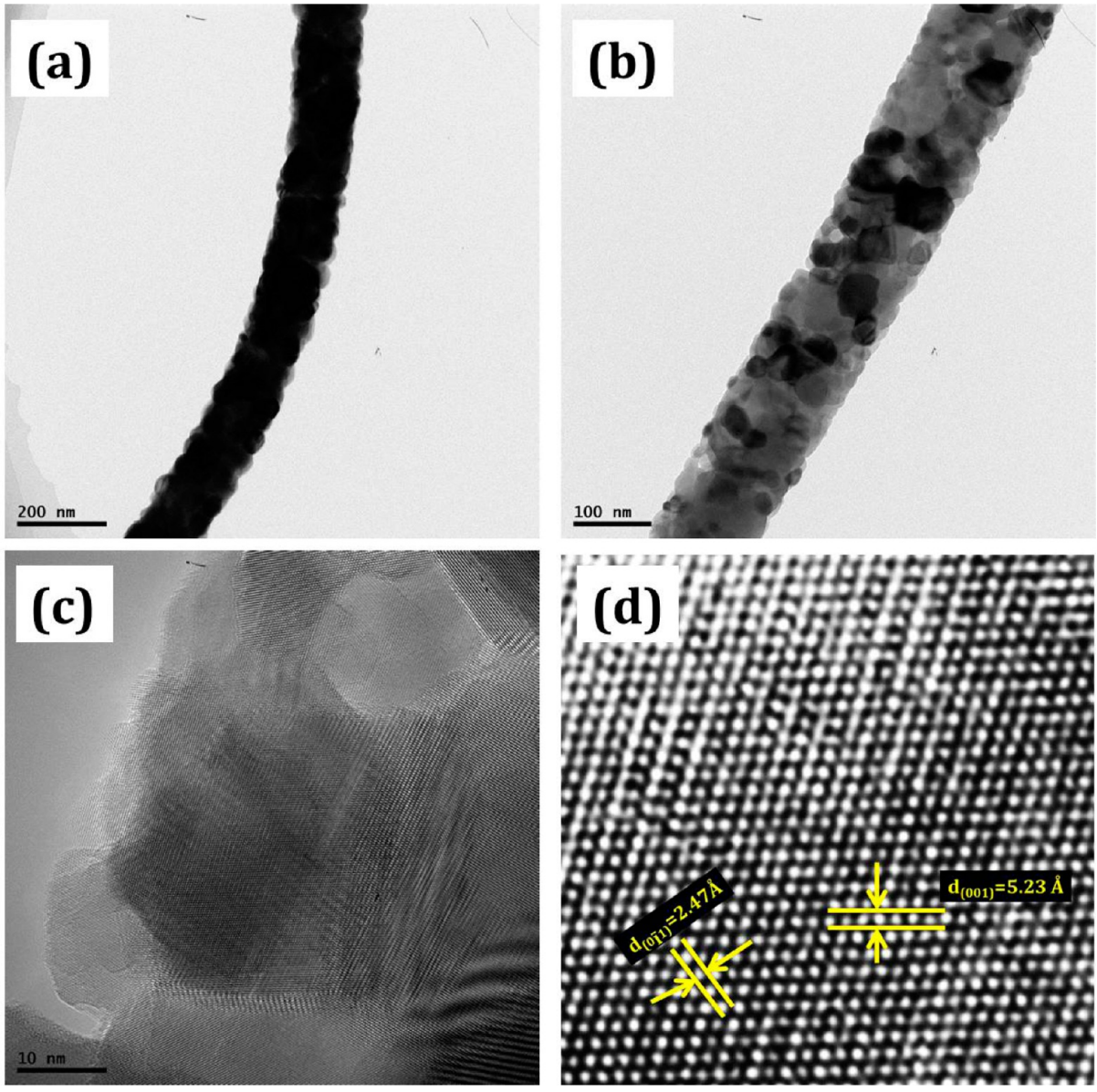

Figure 3. (a, b) TEM and (c, d) HR-TEM images of ZnO mesoporous nanofibers after calcination at 520 °C for 1 h.

samples were further calcined at 520 °C for 1 h. Figure 2(c,d) shows FESEM images of calcined ZnO nanofibers. At a glance, it is clear that the diameters of nanofibers have been decreased up to 160 nm due to removal of the PVP binder and crystallization of ZnO nanofibers. However, it is also noted that the structure of the nanofibers remained the same and continuous. The higher magnified FESEM image reveals that the nanofibers are made up of a number of small mesoporous ZnO nanoparticles. In order to investigate individual single grains of ZnO nanofibers, HRTEM analysis was carried out. Figure 3(a,b) shows TEM micrographs of individual ZnO single nanofibers at different magnifications. The ZnO nanofibers with diameters of 160 nm and lengths from hundreds of nanometers to several micrometres have been observed. After calcination at 520 °C for 1 h, the ZnO mesoporous nanofibers were composed of multi-layered nanoparticles with sizes ranging from 25 to 35 nm. The growth directions for the nanofibers were determined from high resolution TEM (HRTEM) as shown in Figure 3(c). Lattice images are clearly observed in Figure 3(c), indicating that ZnO single grains are highly crystalline. The lattice spacing along the $(0\bar{1}1)$ and (001) planes indicated by yellow lines are found 2.47 Å and 5.23 Å, respectively, which is consistent with the wurtzite crystal structure of ZnO (Figure 3(d)).

Figure 4 shows the TGA curves of PVP−ZnO and pure PVP nanofibers. PVP−ZnO nanofibers exhibited a three-step process of weight loss, with a total weight loss of 80.9%. The weight loss is a function of temperature: 15.445% loss from room temperature to 250 °C, followed by 45.4% between 250 and 473 °C, and finally, a loss of 12.3% that started at about 473 °C and ended at about 720 °C. The first step can be attributed to the loss of volatile solvent. The second significant weight loss can be attributed to loss by the oxidation of sulfides, and PVP chains are decomposed thermally. Over about 720 °C, there is only a slight weight loss up to 1000 °C, and it is expected that the only material changes that occur at this stage are in the crystal structure. It is clear from the TGA curve that the PVP and organic group were completely removed at 720 °C. The weight loss of pure PVP nanofibers began to occur at approximately 342 °C and was complete at about 483 °C. The

dx.doi.org/10.1021/sc400153j | ACS Sustainable Chem. Eng. 2013, 1, 1207−1213

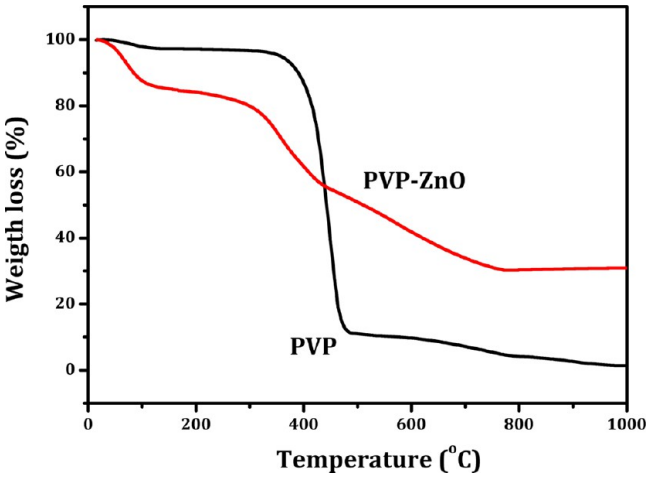

Figure 4. Thermogravimetric analysis (TGA) curves of PVP−ZnO nanofibers. Pure PVP nanofiber (black line) and (b) PVP−ZnO nanofibers (red line).

higher thermal stability of PVP−ZnO nanofibers might be attributed to the higher chain compactness due to the interaction between the PVP and ZnO materials.

The Raman spectrum of ZnO nanofibers was recorded using micro-Raman spectrometer at room temperature. Figure 5

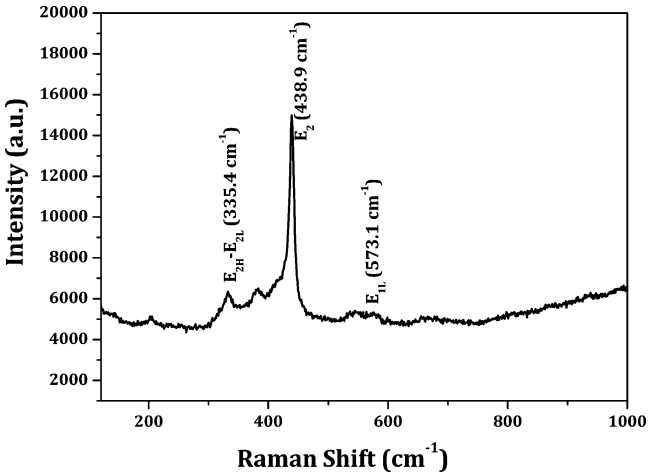

Figure 5. Raman spectrum of ZnO nanofibers.

shows the micro-Raman spectrum of ZnO nanofibers calcined at 520 °C. Raman signals are sensitive to crystal structures and defects. A dominant sharp peak was observed at 438.93 cm^{-1}, which is the characteristic of hexagonal wurtzite ZnO. This shows the Raman-active optical phonon mode, E_2.[36] Other small peaks were also observed at 331.2 cm^{-1} and 573.33 cm^{-1}. The broad peak at 331.2 cm^{-1} is due to multiple phonon scattering,[37] and the peak at 573.33 cm^{-1} is observed due to structural defects like oxygen deficiency. The intensity of the peak at 438.9 cm^{-1} as compared to other peaks is high, which indicates high crystal quality,[38,39] and this result is consistent with the XRD.

The chemical composition of ZnO nanofibers is investigated by XPS analysis, and the results are shown in Figure 6. Figure 6(a) shows the high resolution scan of $Zn(2p_{1/2})$ and $Zn(2p_{3/2})$ peaks for the ZnO nanofibers. The peaks at about 1026.48 and 1049.96 eV confirm that the Zn element exists mainly in the form of the Zn^{2+} chemical state on the sample surface. Figure

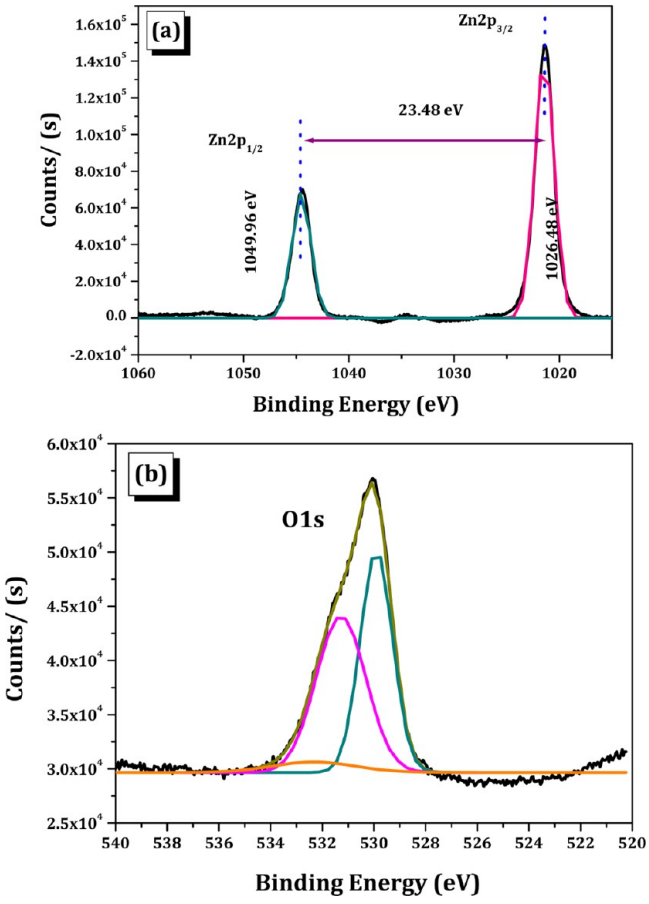

Figure 6. (a) Zn 2p and (b) O1s high resolution XPS scan of ZnO nanofibers.

6(b) shows the high resolution scan of the O 1s peak. The O 1s main peak at 531.70 eV is assigned to the metallic oxides.[40] It is shown that the O 1s peak is somewhat asymmetric, suggesting that there are at least two kinds of oxygen species on the sample surface. The fitting deconvoluted peak with O1S (529.7 eV) is closely related with the oxygen lattice of ZnO. Photoelectrochemical performance, DSSC and QDSSCs device fabrication, and testing of ZnO nanofibers are currently underway in our laboratory.

CONCLUSIONS

In conclusion, we have successfully synthesized mesoporous ZnO nanofibers by a simple and cost-effective electrospinning technique. As-synthesized PVP−ZnO nanofibers have smooth surfaces with diameters of about 400 nm and lengths up to several hundreds of micrometers. The calcination process is beneficial for the formation of highly crystalline ZnO nanofibers. The diameter of calcined samples of ZnO nanofibers have been decreased up to 160 nm due to removal of the PVP binder and crystallization of ZnO nanofibers. These results indicate that electrospinning is an excellent technique for synthesis of long ZnO nanofibers. In the electrospinning process, the PVP is used to adjust the solution viscosity, and ethanol was added to dissolve the PVP and to facilitate solvent evaporation during the electrospinning process. The XRD and HRTEM results reveal that the synthesized ZnO nanofibers have a wurzite crystal structure with excellent crystallinity. The Raman result reveals that the synthesized ZnO nanofibers have

dx.doi.org/10.1021/sc400153j | ACS Sustainable Chem. Eng. 2013, 1, 1207−1213

strong absorption bands at 438.93 cm^{-1}, which is the characteristic of hexagonal wurtzite ZnO.

AUTHOR INFORMATION

Corresponding Author

*E-mail: hongck@chonnam.ac.kr.

Notes

The authors declare no competing financial interest.

ACKNOWLEDGMENTS

This study was financially supported by Chonnam National University 2010.

REFERENCES

(1) Law, M.; Greene, L. E.; Johnson, J. C.; Saykally, R.; Yang, P. Nanowire dye-sensitized solar cells. *Nat. Mater.* **2005**, *4*, 455−459.

(2) Seol, M.; Kim, H.; Taka, Y.; Yong, K. Novel nanowire array based highly efficient quantum dot sensitized solar cell. *Chem. Commun.* **2010**, *46*, 5521−5523.

(3) Vanalakar, S. A.; Mali, S. S.; Pawar, R. C.; Tarwal, N. L.; Moholkar, A. V.; Kim, J. H.; Patil, P. S. Photoelectrochemical properties of CdS sensitized ZnO nanorod arrays: Effect of nanorod length. *J. Appl. Phys.* **2012**, *112*, 044302−044308.

(4) Vanalakar, S. A.; Pawar, R. C.; Suryawanshi, M. P.; Mali, S. S.; Dalavi, D. S.; Moholkar, A. V.; Sim, K. U.; Kown, Y. B.; Kim, J. H.; Patil, P. S. Low temperature aqueous chemical synthesis of CdS sensitized ZnO nanorods. *Mater. Lett.* **2011**, *65*, 548−551.

(5) Pawar, R. C.; Shaikh, J. S.; Babar, A. A.; Dhere, P. M.; Patil, P. S. Aqueous chemical growth of ZnO disks, rods, spindles and flowers: pH dependency and photoelectrochemical properties. *Sol. Energy* **2011**, *85*, 1119−1127.

(6) Park, J. Y.; Kim, J. J.; Kim, S. S. Electrical transport properties of ZnO nanofibers. *Microelectron. Eng.* **2013**, *101*, 8−11.

(7) Ozgur, U.; Alivov, Y. I.; Liu, C.; Teke, A.; Reshchikov, M. A.; Dogan, S.; Avrutin, V.; Cho, S. J.; Morkoc, H. A comprehensive review of ZnO materials and devices. *J. Appl. Phys.* **2005**, *98*, 041301−041403.

(8) Tang, H.; Prasad, K.; Sanjines, R.; Schmid, P. E.; Levy, F. Electrical and optical properties of TiO_2 anatase thin films. *J. Appl. Phys.* **1994**, *75*, 2042−2047.

(9) Bae, H. S.; Yoon, M. H.; Kim, J. H.; Im, S. Photodetecting properties of ZnO-based thin-film transistors. *Appl. Phy. Lett.* **2003**, *83*, 5313−5315.

(10) Wu, J. J.; Chen, G. R.; Lu, C. C.; Wu, W. T.; Chen, J. S. Performance and electron transport properties of TiO_2 nanocomposite dye-sensitized solar cells. *Nanotechnology* **2008**, *19*, 105702.

(11) Noack, V.; Weller, H.; Eychmuller, A. Electron transport in particulate ZnO electrodes: A simple approach. *J. Phys. Chem. B* **2002**, *106*, 8514−8523.

(12) Look, D. C.; Hemsky, J. W.; Sizelove, J. R. Residual native shallow donor in ZnO. *Phys. Rev. Lett.* **1999**, *82*, 2552−2555.

(13) Wang, L.; Zhang, X.; Zhao, S.; Zhou, G.; Zhou, Y.; Qi, J. Synthesis of well-aligned ZnO nanowires by simple physical vapor deposition on c-oriented ZnO thin films without catalysts or additives. *Appl. Phys. Lett.* **2005**, *86*, 024108−0244110.

(14) Bhachu, D. S.; Sankar, G.; Parkin, I. P. Aerosol assisted chemical vapor deposition of transparent conductive zinc oxide films. *Chem. Mater.* **2012**, *24*, 4704−4710.

(15) Look, D. C.; Reynolds, D. C.; Litton, C. W.; Jones, R. L.; Eason, D. B.; Cantwell, G. Characterization of homoepitaxial p-type ZnO grown by molecular beam epitaxy. *Appl. Phys. Lett.* **2002**, *81*, 1830−1832.

(16) Falyouni, F.; Benmamas, L.; Thiandoume, C.; Barjon, J.; Lusson, A.; Galtier, P.; Sallet, V. Metal organic chemical vapor deposition growth and luminescence of ZnO micro-and nanowires. *J. Vac. Sci. Technol., B: Microelectron. Nanometer Struct.–Process., Meas., Phenom.* **2009**, *27*, 1662−1666.

(17) Fouad, O. A.; Ismail, A. A.; Zaki, Z. I.; Mohamed, R. M. Zinc oxide thin films prepared by thermal evaporation deposition and its photocatalytic activity. *Appl. Catal., B* **2006**, *62*, 144−149.

(18) Tarwal, N. L.; Jadhav, P. R.; Vanalakar, S. A.; Kalagi, S. S.; Pawar, R. C.; Shaikh, J. S.; Mali, S. S.; Dalavi, D. S.; Shinde, P. S.; Patil, P. S. Photoluminescence of zinc oxide nanopowder synthesized by a combustion method. *Powder Technol.* **2011**, *208*, 185−188.

(19) Pawar, R. C.; Shaikh, J. S.; Moholkar, A. V.; Pawar, S. M.; Kim, J. H.; Patil, J. Y.; Suryavanshi, S. S.; Patil, P. S. Surfactant assisted low temperature synthesis of nanocrystalline ZnO and its gas sensing properties. *Sens. Actuators, B* **2010**, *151*, 212−218.

(20) Sun, K.; Wei, W.; Ding, Y.; Jing, Y.; Wang, Z. L.; Wang, D. Crystalline ZnO thin film by hydrothermal growth. *Chem. Commun.* **2011**, *47*, 7776−7778.

(21) Pradel, K. C.; Wu, W.; Zhou, Y.; Wen, X.; Ding, Y.; Wang, Z. L. Piezotronic effect in solution-grown p-type ZnO nanowires and films. *Nano Lett.* **2013**, *13*, 2647−2653.

(22) Ashraf, S.; Jones, A. C.; Bacsa, J.; Steiner, A.; Chalker, P. R.; Beahan, P.; Hindley, O. S. R.; Williams, P. A.; Heys, P. N. MOCVD of vertically aligned ZnO nanowires using bidentate ether adducts of dimethylzinc. *Chem. Vap. Deposition* **2011**, *17*, 45−53.

(23) Protasova, L. N.; Rebrov, E. V.; Choy, K. L.; Pung, S. Y.; Engels, V.; Cabaj, M.; Wheatley, A. E. H.; Schouten, J. C. ZnO based nanowires grown by chemical vapour deposition for selective hydrogenation of acetylene alcohols. *Catal. Sci. Technol.* **2011**, *1*, 768−777.

(24) Wang, L.; Zhang, X.; Zhao, S.; Zhou, G.; Zhou, Y.; Qi, J. Synthesis of well-aligned ZnO nanowires by simple physical vapor deposition on c-oriented ZnO thin films without catalysts or additives. *Appl. Phys. Lett.* **2005**, *86*, 024108−024110.

(25) Tien, L. C.; Pearton, S. J.; Norton, D. P.; Ren, F. Synthesis and microstructure of vertically aligned ZnO nanowires grown by high-pressure-assisted pulsed-laser deposition. *J. Mater. Sci.* **2008**, *43*, 6925−6932.

(26) Kitamura, K.; Yatsui, T.; Ohtsu, M.; Yi, G. C. Fabrication of vertically aligned ultrafine ZnO nanorods using metalorganic vapor phase epitaxy with a two-temperature growth method. *Nanotechnology* **2008**, *19*, 175305−175307.

(27) Wang, J. S.; Yang, C. S.; Chen, P. I.; Su, C. F.; Chen, W. J.; Chiu, K. C.; Chou, W. C. Catalyst-free highly vertically aligned ZnO nanoneedle arrays grown by plasma-assisted molecular beam epitaxy. *Appl. Phys. A: Mater. Sci. Process.* **2009**, *97*, 553−557.

(28) Yu, D.; Trad, T.; McLeskey, J. T., Jr.; Craciun, V.; Taylor, C. R. ZnO nanowires synthesized by vapor phase transport deposition on transparent oxide substrates. *Nanoscale Res. Lett.* **2010**, *5*, 1333−1339.

(29) Kevin, M.; Fou, Y. H.; Wong, A. S. W.; Ho, G. W. A novel maskless approach towards aligned, density modulated and multi-junction ZnO nanowires for enhanced surface area and light trapping solar cells. *Nanotechnology* **2010**, *21*, 315602−315610.

(30) Jean, J.; Chang, S.; Brown, P. R.; Cheng, J. J.; Rekemeyer, P. H.; Bawendi, M. G.; Gradecak, S.; Bulovic, V. ZnO nanowire arrays for enhanced photocurrent in PbS quantum dot solar cells. *Adv. Mater.* **2013**, *25*, 2790−2796.

(31) Zhu, Z.; Zhang, L.; Howe, J. Y.; Liao, Speidel, Y. J. T.; Smith, S.; Fong, H. Aligned electrospun ZnO nanofibers for simple and sensitive ultraviolet nanosensors. *Chem. Commun.* **2009**, 2568−2570.

(32) Jung, Y. H.; Park, K. H.; Oh, J. S.; Kim, D. H.; Hong, C. K. Effect of TiO_2 rutile nanorods on the photoelectrodes of dye-sensitized solar cells. *Nanoscale Res. Lett.* **2013**, *8*, 37−42.

(33) Li, D.; Xia, Y. Fabrication of titania nanofibers by electrospinning. *Nano Lett.* **2003**, *3*, 555−560.

(34) Shin, M.; Hohman, M. M.; Brenner, M. P.; Rutledge, G. C. Electrospinning: A whipping fluid jet generates submicron polymer fibers. *Appl. Phys. Lett.* **2001**, *78*, 1149−1151.

(35) Zhou, Y. L.; Zhou, W.-H.; Li, M.; Du, Y.-F.; Wu, S.-X. *J. Phys. Chem. C* **2011**, *115*, 19632−19639.

(36) Wahab, R.; Ansari, S. G.; Kim, Y. S.; Seo, H. K.; Kim, G. S.; Khang, G.; Shin, H.-S. Low temperature solution synthesis and

characterization of ZnO nano-flowers. *Mater. Res. Bull.* **2007**, *42*, 1640−1648.
(37) Ahmad, M.; Pan, C.; Gan, L.; Nawaz, Z.; Zhu, J. Highly sensitive amperometric cholesterol biosensor based on Pt-incorporated fullerene-like ZnO nanospheres. *J. Phys. Chem. C* **2010**, *114*, 243−250.
(38) Qiu, Y.; Yan, K.; Deng, H.; Yang, S. Secondary branching and nitrogen doping of ZnO nanotetrapods: Building a highly active network for photoelectrochemical water splitting. *Nano Lett.* **2012**, *12*, 407−413.
(39) Sharma, S. K.; Rammohan, A.; Sharma, A. Templated one step electrodeposition of high aspect ratio n-type ZnO nanowire arrays. *J. Colloid Interface Sci.* **2010**, *344*, 1−9.
(40) Atanasova, G.; Og Dikovska, A.; Stankova, M.; Stefanov, P.; Atanasov, P. A. XPS study of ZnO nanostructures prepared by laser ablation. *J. Phys.: Conf. Ser.* **2012**, *356*, 012036−012041.